Combinatorial hydrogel library enables identification of materials that mitigate the foreign body response in primates

Citation: Vegas, Arturo J; Veiseh, Omid; Doloff, Joshua C; Ma, Minglin; Tam, Hok Hei; Bratlie, Kaitlin; Li, Jie, et al. "Combinatorial Hydrogel Library Enables Identification of Materials That Mitigate the Foreign Body Response in Primates." Nature Biotechnology 34, no. 3 (January 2016): 345–352. © 2016 Nature America, Inc

As Published: http://dx.doi.org/10.1038/nbt.3462

Publisher: Nature Publishing Group

Persistent URL: http://hdl.handle.net/1721.1/109048

Version: Author's final manuscript: final author's manuscript post peer review, without publisher's formatting or copy editing

HHS Public Access

Author manuscript

Nat Biotechnol. Author manuscript; available in PMC 2016 July 25.

Published in final edited form as:

Nat Biotechnol. 2016 March ; 34(3): 345–352. doi:10.1038/nbt.3462.

Combinatorial hydrogel library enables identification of materials that mitigate the foreign body response in primates

Arturo J Vegas[1,2,12], **Omid Veiseh**[1,3], **Joshua C Doloff**[1,2], **Minglin Ma**[1,2,12], **Hok Hei Tam**[1,3], **Kaitlin Bratlie**[1,3,12], **Jie Li**[1,2], **Andrew R Bader**[1,2,12], **Erin Langan**[1,2], **Karsten Olejnik**[1,2], **Patrick Fenton**[1,2], **Jeon Woong Kang**[4], **Jennifer Hollister-Locke**[5], **Matthew A Bochenek**[6], **Alan Chiu**[1,2], **Sean Siebert**[1,2], **Katherine Tang**[1,2], **Siddharth Jhunjhunwala**[1,2], **Stephanie Aresta-Dasilva**[1,2], **Nimit Dholakia**[1,2], **Raj Thakrar**[1,2], **Thema Vietti**[1,2], **Michael Chen**[1,2], **Josh Cohen**[5], **Karolina Siniakowicz**[5], **Meirigeng Qi**[6], **James McGarrigle**[6], **Adam C Graham**[7], **Stephen Lyle**[8], **David M Harlan**[9], **Dale L Greiner**[9], **Jose Oberholzer**[6], **Gordon C Weir**[5], **Robert Langer**[1,2,3,10,11], and **Daniel G Anderson**[1,2,3,10,11]

[1]David H Koch Institute for Integrative Cancer Research, Massachusetts Institute of Technology, Cambridge, Massachusetts, USA

[2]Department of Anesthesiology, Boston Children's Hospital, Boston, Massachusetts, USA

[3]Department of Chemical Engineering, Massachusetts Institute of Technology, Cambridge, Massachusetts, USA

[4]MIT Spectroscopy Lab, Massachusetts Institute of Technology, Cambridge, Massachusetts, USA

[5]Section on Islet Cell and Regenerative Biology, Research Division, Joslin Diabetes Center, Boston, Massachusetts, USA

[6]Department of Surgery, Division of Transplantation, University of Illinois at Chicago, Chicago, Illinois, USA

[7]Center for Nanoscale Systems, Harvard University, Cambridge, Massachusetts, USA

[8]Department of Cancer Biology, University of Massachusetts Medical School, Worcester, Massachusetts, USA

Correspondence should be addressed to D.G.A. (dgander@mit.edu).

[12]Present addresses: Department of Chemistry, Boston University, Boston, Massachusetts, USA (A.J.V.); Department of Biological and Environmental Engineering, Cornell University, Ithaca, New York, USA (M.M.); Department of Materials Science and Engineering, Iowa State University, Ames, Iowa, USA, and Department of Chemical and Biological Engineering, Iowa State University, Ames, Iowa, USA (K.B.); Department of Mechanical Engineering, Massachusetts Institute of Technology, Cambridge, Massachusetts, USA (A.R.B.).

Note: Any Supplementary Information and Source Data files are available in the online version of the paper.

AUTHOR CONTRIBUTIONS

A.J.V., O.V., J.C.D., M.M., K.B., J.L., A.R.B., E.L., K.O., P.F., J.W.K., J.H.-L., M.A.B., A.C., S.S., K.T., S.J., S.A.-D., N.D., R.T., T.V., M.C., J.C., K.S., M.Q. and J.M. designed and performed experiments, and analyzed data. H.H.T. assisted with data processing and data presentation. A.C.G. assisted with SEM imaging. S.L. assisted with histology. D.M.H., D.L.G., J.O. and G.C.W. provided conceptual advice and technical support. A.J.V. and D.G.A. wrote the paper. R.L. and D.G.A. supervised the study. All authors discussed the results and commented on the manuscript.

COMPETING FINANCIAL INTERESTS

The authors declare competing financial interests: details are available in the online version of the paper.

[9]Diabetes Center of Excellence, University of Massachusetts Medical School, Worcester, Massachusetts, USA

[10]Institute for Medical Engineering and Science, Massachusetts Institute of Technology, Cambridge, Massachusetts, USA

[11]Division of Health Science Technology, Massachusetts Institute of Technology, Cambridge, Massachusetts, USA

Abstract

The foreign body response is an immune-mediated reaction that can lead to the failure of implanted medical devices and discomfort for the recipient[1–6]. There is a critical need for biomaterials that overcome this key challenge in the development of medical devices. Here we use a combinatorial approach for covalent chemical modification to generate a large library of variants of one of the most widely used hydrogel biomaterials, alginate. We evaluated the materials *in vivo* and identified three triazole-containing analogs that substantially reduce foreign body reactions in both rodents and, for at least 6 months, in non-human primates. The distribution of the triazole modification creates a unique hydrogel surface that inhibits recognition by macrophages and fibrous deposition. In addition to the utility of the compounds reported here, our approach may enable the discovery of other materials that mitigate the foreign body response.

The foreign body response to implanted biomaterials consists of inflammatory events and wound-healing processes[1] that lead to fibrosis. The cellular and collagenous deposition isolate the device from the host[1,7,8]. This can interfere with sensing of the host environment, lead to painful tissue distortion, cut off nourishment (for implants containing living, cellular components) and ultimately lead to device failure[1,3]. Overcoming the foreign body response to implanted devices could pave the way for implementing new medical advances, making the development of materials with both anti-inflammatory and antifibrotic properties a critical medical need[1,2,4]. Macrophages are a key component of material recognition and actively adhere to the surface of foreign objects[1,3,5,9,10]. Objects too large for macrophage phagocytosis initiate processes that result in the fusion of macrophages into foreign-body giant cells[1,3]. These multinucleated bodies amplify the immune response by secreting cytokines and chemokines that result in the recruitment of fibroblasts that actively deposit matrix to isolate the foreign material[1,3,11,12]. This response has been described for materials that encompass a wide range of physicochemical properties, from naturally occurring polymers to synthetic materials[3,9,13].

Alginate is a unique and versatile biomaterial that forms hydrogels in di-cationic aqueous solutions (Ca^{2+}, Ba^{2+}) and has been used in numerous biomedical applications including drug delivery, tissue regeneration, implantable sensors and cell encapsulation[14,15]. Its low cost, low toxicity, mild gelation (harmless to cells) and tunability has made alginate a popular coating in biomedical device research and the most commonly used material for encapsulation technologies[14]. The immune recognition of alginate microspheres results in even empty microspheres eliciting a foreign body response, and the presence of encapsulated allogeneic or xenogeneic donor tissue can further stimulate this response[16–25]. The fibrotic response to alginate has been observed in non-human primate (NHP) models,

and the fibrosis of alginate microspheres in rodents has been shown to be strain dependent[26,27]. Implantation of alginate microcapsules in the intraperitoneal space of rodent models characterized as immune compliant (e.g., BALB/c) yields implants relatively free of fibrous deposition[26,27], but in C57BL/6J mice, microcapsules are covered with fibrous overgrowth, mimicking the foreign body response observed in humans and non-human primates[21,22,26]. Here we develop a large combinatorial library of hydrogels to identify materials with reduced immune recognition in preclinical fibrosis models, C57BL/6J mice and non-human primates.

Previous combinatorial approaches have developed materials for reducing biofouling and fibroblast activation[28,29], but to our knowledge there have been no reports of combinatorial development of materials for mitigating foreign body responses. The physicochemical parameters governing anti-fibrotic properties are not fully understood, making rationally designed approaches challenging[4,6]. We developed a combinatorial biomaterial approach to generate a library of alginate-based hydrogels, using several diverse chemical reactions that covalently modify latent functionalities and properties on the polymeric alginate backbone (Supplementary Note and Supplementary Fig. 1). We used low molecular weight (MW), ultrapure alginate VLVG with high guluronate (G) content (>60% G, ∼25 kDa MW, NovaMatrix) as the starting material and synthesized a 774-membered alginate analog library with a variety of amines, alcohols, azides and alkynes (Fig. 1a). Of the 774 alginate analogs, 35 analogs resulted in unacceptably low yields (<20%) and 634 alginates were determined to be capable of gelation after chemical modification (Fig. 1c). These alginates were then evaluated as bulk hydrogels *in vivo*, using a rapid subcutaneous mouse model to measure levels of acute inflammation (Fig. 1b)[30]. This assay monitors inflammation subcutaneously with an imaging agent which yields increased fluorescence in response to increased cathepsin activity, a marker for immune cell activation[31,32]. Two hundred analogs displayed fluorescent levels that were lower than the unmodified, ultrapure VLVG alginate (Fig. 1c), and we verified that fluorescence levels were not artificially suppressed by the presence of barium in our implants (Supplementary Fig. 2a).

Because microcapsules are the preferred alginate geometry in multiple applications[14,18], we took the 16 top-performing polymers and an additional 53 structurally diverse analogs represented in the top 200 (Supplementary Table 1) and fabricated them into barium-alginate microcapsules, previously demonstrated to have long-term *in vivo* stability[17,33,34]. These microcapsules had diameters of 300 to 350 μm (a size at which alginate induces strong foreign body responses[35]), and were evaluated subcutaneously one material per mouse (Fig. 1d,e). Of the 69 formulated alginate microcapsules (Supplementary Table 1), we found several polymers with reduced cathepsin activity *in vivo* (Fig. 1e). We sampled the implant sites of the top ten alginates 28 d after implantation. Masson's trichrome (MT) staining of tissue sections showed that three modified alginates, Z2-Y12, Z1-Y15 and Z1-Y19, produced microcapsules with lower fibrotic overgrowth over the implant (Fig. 1f; hematoxylin and eosin staining, Supplementary Fig. 2b). Quantification of the relative collagen density (blue pixel density) shows that these lead materials have lower collagen levels at the implant surface compared to the control microcapsules (Fig. 1g). To test if our results in the subcutaneous space translate to other implantation sites, we implanted microcapsules in the intraperitoneal space of C57BL/6J mice (Fig. 2). The top ten lead

modified alginates show varying degrees of fibrosis after 14 d, with the modified alginates Z2-Y12, Z1-Y15 and Z1-Y19 showing almost no fibrous deposition. All three of these lead materials contained a triazole functionality, the product of a Huisgen cycloaddition between azides and alkynes (Fig. 2e). Triazole-containing modifications associated with improved *in vivo* performance overall, with principal component functional group analysis of all 634 modified alginates clustering the 34 triazole-modified alginates from the 69 modified alginates selected for secondary screening, the 4 triazole alginates represented in the top 10 performers, and the 3 lead triazole alginates (Supplementary Fig. 2c). Both Z1-Y15 and Z1-Y19 also share the same PEG-azide linker whereas Z2-Y12 bears the more hydrophobic benzyl Z2 linker. Both Z2-Y12 and Z1-Y15 share six-membered heterocyclic end groups whereas Z1-Y19 bears an amine-substituted aromatic ring. Despite these similarities Z1-Y15 bears a more hydrophilic triazole-thiomorpholine dioxide functionality versus the more hydrophobic triazole-tetrahydrofuran of Z2-Y12 and triazole-aniline of Z1-Y19, suggesting triazole modifications may be a versatile chemical space for designing biomaterials that can mitigate foreign body responses.

Cellular staining and confocal microscopy of the Z2-Y12, Z1-Y15 and Z1-Y19 microcapsules showed little to no presence of macrophages (CD68), myofibroblasts (α-smooth muscle actin, SMA) or general cellular deposition (DAPI) (Fig. 2b). The conventional microcapsule alginate, however, showed substantial quantities of these cell populations on the retrieved microcapsules. We found lower levels of SMA and collagen[36] in Z2-Y12, Z1-Y15, Z1-Y19 as compared to the control microcapsules (Fig. 2c,d). To determine if cellular toxicity was a contributing factor, we tested microcapsules of our formulated lead materials in a cellular viability assay (CellTiter Glo) with murine macrophage RAW 264.7 cells (Supplementary Fig. 2e), but found no appreciable cellular toxicity. Z2-Y12 microcapsules showed the lowest cytokine levels and Z2-Y12, Z1-Y15 and Z1-Y19 microcapsules had lower levels of TNF-α and IL-4 as compared to SLG20 controls (Supplementary Fig. 2f). Quantification of 79 RNA sequences of known inflammation factors and immune cell markers isolated from retrieved Z2-Y12 microcapsules also provides evidence of lower levels of inflammation for these implants (Supplementary Fig. 3). The expression profile from the surrounding intraperitoneal fluid and fat tissue of the implanted microcapsules did not show significantly different profiles. In addition, no enrichment for any specific macrophage subtype was observed between Z2-Y12 and control microcapsules. To confirm that these results were not related to varied levels of contamination or incomplete alginate purification, we characterized control and the three lead alginate microcapsules for endotoxin, glucan, flagellin and lipoteichoic acid (LTA), a pathogen-associated molecular pattern that has previously been associated with incomplete alginate purification (Supplementary Fig. 4)[18,37–43]. No detectable amounts of any of these contaminants were measured in our control or lead material microcapsules.

We performed FACS analysis on retrieved microcapsules after 14 d in the intraperitoneal space and found that Z2-Y12, Z1-Y15 and Z1-Y19 microcapsules displayed substantially lower cell numbers of macrophage and neutrophil populations (Fig. 3a and Supplementary Fig. 5a–d). To see if lower macrophage recruitment was evident *in vivo*, we performed intraperitoneal intravital imaging 7 d after implantation of fluorescent Z2-Y12 microcapsules in transgenic MAFIA mice (where macrophages express GFP) (Fig. 3b and

Supplementary Videos 1 and 2). Z2-Y12 microcapsules showed much lower levels of macrophages and no visible macrophage aggregation, in contrast to SLG20 microcapsules.

The lack of immune cell recruitment and/or activation to the surface of Z2-Y12, Z1-Y15 and Z1-Y19 microcapsules indicates that the chemical modification of the polymer chains may be creating distinctive surfaces. We performed confocal Raman spectroscopic mapping to determine the distribution of the Z2-Y12, Z1-Y15 and Z1-Y19 chemical modifications in the microcapsules (Fig. 3c and Supplementary Fig. 6a,b). Notably, the diagnostic Raman signature for the tetrahydropyran of Z2-Y12 and the thiomorpholine of Z1-Y15 had a higher intensity at the surface of the microcapsule than at the core. The aniline of Z1-Y19 showed a uniform distribution throughout the microcapsule cross-section, but modification at the surface was also present. We then performed freeze-fracture cryo-scanning electron microscopy (cryo-SEM) on Z2-Y12, Z1-Y15, and Z1-Y19 microcapsules to examine both the surface and core topography of our alginate-analog microspheres compared to controls (Fig. 3d). The three lead microcapsules displayed a more variable porosity throughout the microcapsule core compared to either the blended control or conventional SLG20 microcapsules, with pores ranging from 1 μm to 10 μm in size (Supplementary Fig. 6c). The surfaces of Z2-Y12 and Z1-Y15 microcapsules showed fewer cratered features, whereas the surface of Z1-Y19 microcapsules appeared coarse (Fig. 3d). These surface differences are likely created by interactions at the boundary layer between the modified polymer chains and the surrounding aqueous solution. Previous studies have established a relationship between the surface porosity of materials like polytetrafluoroethylene (PTFE) and angiogenesis, with larger pore sizes of PTFE inducing more angiogenesis than PTFE with smaller pore sizes[44,45]. However, in our studies the three lead and control materials possess comparable porosities (Supplementary Fig. 6c), but still display different surface topographies (Fig. 3d). Polymer modification levels between 14–25% were measured for the different lead materials using elemental analysis (Fig. 3e). Using profilometry only Z1-Y19 microcapsules yielded surfaces with a markedly higher surface roughness (Pa) than controls and the other lead material microcapsules (Fig. 3e). No trend was observed between these roughness measurements and host responses, in contrast to other reports[46]. We next evaluated whether these lead materials gave rise to spheres with altered mechanical properties by determining their Young's modulus (Fig. 3e)[47]. The modulus for the lead materials was similar to the modulus of the control alginates and showed no trend with the biological responses characterized for each material (Fig. 3e). Protein adsorption differences have been previously described with cation-coated alginate microcapsules[48]. We determined if these lead materials had anti-fouling properties by quantifying protein levels adsorbed to the material surface after incubation with fetal bovine serum. Lower protein levels were measured between the lead materials and SLG20 surfaces, but protein adsorption between lead and V/S surfaces were comparable.

To further evaluate performance of our lead combinatorial-modified materials, we tested our three lead materials Z2-Y12, Z1-Y15 and Z1-Y19 in a non-human primate model of fibrosis. Spheres with narrowly distributed 1.5-mm diameters of SLG20 and Z2-Y12, Z1-Y15 and Z1-Y19 materials were separately implanted intraperitoneally into non-human primates (n = 3 each) using a minimally invasive laparoscopic procedure[49]. We retrieved the spheres by intraperitoneal lavage (Supplementary Video 3) and biopsied omental tissue at 4 weeks, with

the Z2-Y12 primate cohort allowed to continue for 6 months. Whereas in our previous report SLG20 spheres with 1.5-mm diameters displayed a reduced foreign body response after 2 weeks in the intraperitoneal space in non-human primates[33], there were among the SLG20 1.5-mm spheres retrieved after 4 weeks in the intraperitoneal space numerous spheres that were fibrosed and clumped together (Fig. 4a). This result indicates that larger sphere size alone is not capable of long-term reduction of foreign body responses in non-human primates. Z2-Y12, Z1-Y15 and Z1-Y19 spheres with 1.5-mm diameters displayed substantially reduced fibrotic responses after 4 weeks in the intraperitoneal space compared to 1.5-mm SLG20 spheres. SLG20 spheres had more extensive immune macrophage and fibrosis-associated activated myofibroblast coverage (Fig. 4b), consistent with the visible fibrotic overgrowth seen in the phase contrast imaging. Z1-Y19 spheres displayed more coverage by macrophage and myofibroblasts than either Z2-Y12 or Z1-Y15, but less compared to SLG20. Z2-Y12 and Z1-Y15 spheres had markedly lower levels of SMA protein as compared to SLG20 spheres (Fig. 4c), but Z1-Y19 spheres did not, despite the lower average SMA measured. Hydroxyproline quantification revealed lower collagen levels for all three lead formulations compared to SLG20 (Fig. 4d). Histological analysis of embedded spheres in the surrounding omental tissue showed a similar trend to the phase-contrast imaging of particles retrieved from the lavage (Supplementary Fig. 7a). MT and HE staining showed that Z1-Y15 and Z1-Y19 spheres displayed thinner fibrotic spheres than SLG20 spheres, and in the case of Z2-Y12 no embedded spheres could be found in the omental tissue at 4 weeks, suggesting spheres did not adhere to the omental tissue due to lack of fibrosis. Z2-Y12 spheres retrieved after 6 months were largely clean (Fig. 4e,f) of fibrotic deposition and showed few associated macrophages or myofibroblasts (Fig. 4f). Interestingly, cells visible on some spheres by confocal imaging do not stain for CD68, CD11b, SMA, Ly6g or F-actin.

Using combinatorial methods we have developed a large library of alginate hydrogels and identified chemical modifications that substantially reduce the inflammatory effects of alginate hydrogels and improve their performance in non-human primates. In these studies, the nature of the chemical modification proved crucial, as bulk properties, such as mechanical stability, surface roughness and protein adsorption, could not explain *in vivo* performance, and larger spheres alone could not mitigate long-term fibrosis in non-human primates. Among the three lead materials, the two (Z2-Y12, Z1-Y15) that displayed enriched surface localization of their modification by confocal Raman also performed better in non-human primates than the one (Z1-Y19) that had a more uniform modification distribution. All three lead modifications were triazole derivatives, which suggests that this class of molecules may modulate immune cell populations at the surface of these materials, specifically macrophages, in a manner that inhibits their activation and disrupts fibrotic processes. To our knowledge, no previous study has evaluated the ability of triazole-containing materials to mitigate foreign body responses. Although there is a small-molecule triazole scaffold currently being investigated as an immunomodulatory agent[50,51], the molecular target of this compound has not been determined and activity is attributed to modulation of cellular signaling in T cells, not macrophages[51]. Triazole surface modification may have broad impact in biomedical applications that use alginate-based materials—such as drug delivery, cell encapsulation, tissue engineering and implantable sensors—or other

implantable materials. We further show the clinical potential of these materials in a related study where one of our lead modified alginates, Z1-Y15, supported long term glycemic correction of immune-competent diabetic mice with encapsulated human stem cell–derived beta cells[52]. Clinical application of these materials is also facilitated by the emergence of methods for terminal sterilization that do not affect hydrogel or modification stability[53,54]. The approach for combinatorial modification and biological evaluation described here provides a general strategy for the identification of materials that can mitigate the foreign body response and improve the long-term performance of implanted products.

ONLINE METHODS

In brief, all materials were implanted subcutaneously or intraperitoneally into and retrieved at specified times from C57BL/6J mice in accordance with approved protocols and federal guidelines. Sample processing, staining, FACS, NanoString expression analysis, and imaging were performed as detailed below. Representative images in all figures are from n = 5 mice or n = 3 non-human primates per treatment group unless specified otherwise. One-way ANOVA with Bonferroni correction was utilized to allow for statistical comparison of multiple means. #P < 0.05, *P < 0.01, ***P < 0.0001, ns = not significant. Quantified data from *in vivo* samples are group mean values ± s.e.m., while quantified data from in vitro experiments are mean values ± s.d.

Statistical analysis

Data are expressed as mean ± s.e.m., and n = 5 for mice and n = 3 for non-human primates per time point and per treatment group, unless specified otherwise. FACS data were analyzed for statistical significance either by unpaired, two-tailed t-test, or one-way ANOVA with Bonferroni multiple comparison correction, unless indicated otherwise, as implemented in GraphPad Prism 5; #P < 0.05, *P < 0.01, **P < 0.001, and ***P < 0.0001. Western blot and collagen quantification assays were analyzed for statistical significance using one-way ANOVA with Bonferroni multiple comparison correction in Origin 8.5, with significance levels specified in the figure captions. High-throughput NanoString-based gene expression data were normalized using the geometric means of the NanoString positive controls and background levels were established using the means of the negative controls. The sum of the housekeeping genes *Tubb5, Hprt1, Bact* and *Cltc* were used to normalize between samples. Data were then log-transformed. For each gene of interest and compartment group, a one-way ANOVA for the effect of material was performed. P-values were computed from pairwise comparisons performed using Tukey's Honest Significant Difference test and the method of Benjamini and Hochberg was used to control the false discovery rate under 0.05. Genes were considered differentially expressed if P < 0.05.

Alginate chemical modification

Alginate amidation—Alginate (Pronova UPVLVG from NovaMatrix, 1 equiv., 100 mg = 0.52 mmol of COOH available for reaction) was dissolved as a 2% alginate solution in a 3:2 water:acetonitrile mixture (5 ml total volume). Amine (N1 to N9, Z1, Z2) (1 equiv., Sigma Aldrich or TCI America) was then added to the mixture along with the coupling agent 2-chloro-4,6-dimethoxy-1,3,5-triazine (CDMT, 0.5 equiv., 45 mg, Sigma Aldrich) and

4-methylmorpholine (NMM, 1 equiv., 56 μl, Sigma Aldrich). The mixture was stirred at 55 °C overnight and the solvent was removed under reduced pressure. The resulting solid was dissolved in water and filtered through cyano-modified silica gel (Silicycle) to remove insoluble precipitate. The resulting solution was then dialyzed against a 10,000 MWCO dialysis membrane overnight with DI water to further purify the polymer. The resulting solution was then lyophilized to get purified compound.

Alginate esterification—Alginate (Pronova UPVLVG from NovaMatrix, 1 equiv., 100 mg = 0.52 mmol of COOH available for reaction) was dissolved as a 2% alginate solution in a 3:2 water:alcohol (O1 to O12) mixture (5 ml total volume). The coupling agent 2-chloro-4,6-dimethoxy-1,3,5-triazine (CDMT, 0.5 equiv., 45 mg, Sigma Aldrich) and 4-methylmorpholine (NMM, 1 equiv., 56 μl, Sigma Aldrich) was then added and the mixture was stirred at 55 °C overnight. The next day the solvent was removed under reduced pressure. The resulting solid was dissolved in water and filtered through cyano-modified silica gel (Silicycle) to remove insoluble precipitate. The resulting solution was then dialyzed against a 10,000 MWCO dialysis membrane overnight with DI water to further purify the polymer. The resulting solution was then lyophilized to get purified compound.

Huisgen cycloaddition ("Click")—In a second step, alginates reacted with Z2 were dissolved in a solution of water: methanol 1:1 (5 ml total). Sodium azide (0.25 equiv, 19 mg, Sigma Aldrich), sodium L-ascorbate (0.05 equiv., 19 mg, Sigma Aldrich), trans-N,N'-dimethylcyclohexane-1,2-diamine (0.25 equiv, typically 20 μl, Sigma Aldrich), copper(I)-iodide (0.5 equiv, 10 mg, Sigma Aldrich) were added as coupling agents. Then 0.51 mmol of the respective alkyne (Y1 to Y20) was added and the mixture was stirred at 55 °C overnight. The solvent was removed under reduced pressure. The resulting solid was dissolved in water and filtered through cyano-modified silica gel to remove insoluble precipitate. The clear solution was lyophilized and dissolved in 5 ml of water and dialyzed. The resulting solution was then dialyzed against a 10,000 MWCO dialysis membrane overnight with DI water to further purify the polymer. The resulting solution was then lyophilized to get purified compound.

In a second step, alginates reacted with Z1 were dissolved in a solution of water: methanol 1:1 (5 ml total). Tris[(1-benzyl-1H-1,2,3-triazol-4-yl) methyl]amine (TBTA, 0.2 equiv, 50 mg, Sigma Aldrich), triethylamine (0.25 equiv., typically 15 μl, Sigma Aldrich), *Copper*(I)-*Iodide* (0.25 equiv, 5 mg, Sigma Aldrich) were added as coupling agents. Then 0.51 mmol of the respective alkyne was added and the mixture was stirred at 55 °C overnight. The solvent was removed under reduced pressure. The resulting solid was dissolved in water and filtered through cyano modified silica gel to remove insoluble precipitate. The clear solution was lyophilized, dissolved in 5 ml of water and dialyzed. The resulting solution was then dialyzed against a 10,000 MWCO dialysis membrane overnight with DI water to further purify the polymer. The resulting solution was then lyophilized to get purified compound.

Optimized syntheses for preparation of Z2-Y12, Z1-Y15 and Z1-Y19

Z2-Y12 amine: 10 g of 2-(2-propynyloxy) tetrahydropyran (1 equiv. 71.36 mmol) was added to a solution of 5.1g sodium azide (1.1 equiv, 78.5 mmol), 1.41 g sodium ascorbate

(0.1 equiv, 7.14 mmol), 2.29 ml trans-N-N′-dimethylcyclohexane-1,2-diamine (0.25 equiv, 17.83 mmol), 3.4 g copper(I)-iodide (0.025 equiv, 17.83 mmol) in 75 ml methanol. To this mixture 19.97 g of 4 iodobenzylamide HCl was added. The reaction was stirred overnight at 55 °C. The solvent was removed under reduced pressure. The crude reaction was purified by liquid chromatography with dichloromethane:ultra (22% MeOH in DCM with 3% NH_4OH) mixture 0% to 40% on silica gel. The product was then reacted with alginate as described below.

Z1-Y15 amine: 3.5 g of 4-propagylthiomorpholine 1,1-dioxide (1 equiv. 20 mmol) was added to a solution of 2.5g TBTA (0.2 equiv, 4 mmol), 750 µl triethylamine (0.5 equiv, 10 mmol), 250 mg copper(I)-iodide (0.06 equiv., 1.3 mmol) in 50 ml methanol. The mixture was cooled to 0 °C and 5.25 ml of 11-azido-3,6,9-trioxaundecan-1-amine (1 equiv, 20 mmol) was added. The reaction was stirred overnight at 55 °C. The solvent was removed under reduced pressure. The crude reaction was purified by liquid chromatography with water: acetonitrile mixture 0% to 100% on a C18 column. The product was then reacted with alginate as described below.

Z1-Y19 amine: 3 g of 4-ethynylaniline (1 equiv., 20.2 mmol) was added to a solution of 2.5 g TBTA (0.2 equiv., 4 mmol), 750 µl triethylamine (0.5 equiv., 10.1 mmol), 250 mg copper(I)-iodide (0.06 equiv, 1.31 mmol) in 50 ml methanol. The mixture was cooled to 0 °C and 5.25 ml of 11-azido-3,6,9-trioxaundecan-1-amine (1 equiv, 20 mmol) was added. The reaction was stirred overnight at 55 °C. The solvent was removed under reduced pressure. The crude reaction was purified by liquid chromatography with dichloromethane:ultra (22% MeOH in DCM with 3% NH_4OH) mixture 0% to 30% on a cyano-functionalized silica column. The product was then reacted with alginate as described below.

Alginate reaction: 1.5 g of VLVG (1 equiv) was dissolved in 45 ml of water and 675 mg of 2-chloro-4,6-dimethoxy-1,3,5-triazine (CDMT, 0.5 equiv) and 840 µl of N-methylmorpholine (NMM, 1 equiv.) was added. Then 7.65 mmol of the Z2-Y12, Z1-Y15, or Z1-Y19 amine was dissolved in 22.5 ml acetonitrile and added to the mixture. The reaction was stirred overnight at 55 °C. The solvent was removed under reduced pressure and the solid was dissolved in water. The solution was filtered through a pad of cyano-functionalized silica and the water was removed under reduced pressure to concentrate the solution. It was then dialyzed against a 10,000 MWCO membrane in DI water overnight. The water was removed under reduced pressure to give the functionalized alginate.

Alginate gelation assay

The gelation of alginate analogs was evaluated using a fluorescence entrapment assay. A volume of 100 µl of a 1% (w/v) solution of alginate was dispensed into the wells of a 96-well opaque plate. A volume of 1 µl of a 1% (w/v) solution of rhodamine B (Sigma-Aldrich, cat#: 83689) in DMSO was then added to each well, followed by addition of 50 µl of a 1 M barium chloride solution. The mixture was incubated for 10 min on an orbital shaker, and then all the excess solution was removed (only hydrogel should remain in the well, if present). The wells were then washed 3 times with 100 µl of deionized water, taking care not

to disturb any hydrogels that have formed in the wells. Fluorescence was then measured using a M200 Tecan plate reader with a gain setting of 52 and an excitation wavelength of 540 nm and an emission wavelength of 580 nm. UPVLVG alginate was used as a positive control, deionized water as a negative control. Analogues yielding fluorescence values greater than 15,000 were classified as competent hydrogels.

Subcutaneous cathepsin measurements of bulk hydrogels

Primary subcutaneous evaluation of the entire alginate analog collection was performed with multiple implantations per mouse as described in Bratlie *et al.*[30] Briefly, 2% (w/w) alginate solutions of each analog were subcutaneously injected into bilateral sites on the dorsal surface of female SHK-1 mice in an eight-array format, 0.8 cm paramedian to the midline and 1 cm between adjacent sites. Alginate solutions were then cross-linked *in situ* with a successive injection of 50 μl of 100 mM calcium chloride solution. Each mouse was implanted with a control unmodified UPVLVG alginate solution to serve as an internal control for fluorescence normalization during 7-d imaging with Prosense.

Microcapsule/sphere formation

All buffers were sterilized by autoclave and alginate solutions were sterilized by filtration through a 0.2 μm filter. After solutions were sterilized, aseptic processing was implemented by performing capsule formation in a type II class A2 biosafety cabinet to maintain sterility of manufactured microcapsules/spheres for subsequent implantation. An electrostatic droplet generator was set up in the biosafety cabinet as follows: an ES series 0–100 kV, 20 Watt high voltage power generator (Gamma ES series, Gamma High Voltage Research, FL, USA) is connected to the top and bottom of a blunt-tipped needle (SAI Infusion Technologies, IL, USA). This needle is attached to a 5 ml luer lock syringe (BD, NJ, USA) which is clipped to a syringe pump (Pump 11 Pico Plus, Harvard Apparatus, MA, USA) that is oriented vertically. The syringe pump pumps alginate out into a glass dish containing a 20 mM barium 5% mannitol solution (Sigma Aldrich, MO, USA). The settings of the PicoPlus syringe pump are 12.06 mm diameter and 0.2 ml/min flow rate. After the capsules are formed, they are then collected and then washed with HEPES buffer (NaCl 15.428 g, KCl 0.70 g, $MgCl_2$*$6H_2O$ 0.488 g, 50 ml of HEPES (1 M) buffer solution (Gibco, Life Technologies, California, USA) in 2 L of DiH_2O) 4 times. The alginate capsules are left overnight at 4 °C. The capsules are then washed 2 times in 0.8% saline and kept at 4 °C until use. The control VLVG/SLG100 (V/S) blend had to receive additional washing, 7 l of 0.8% saline over a period of 7 d, due to a high quantity of initial barium release in this formulation (this barium release was not observed for any other formulation as monitored using inductively coupled plasma atomic emission spectroscopy, ICP-AES).

To solubilize alginates, SLG20 (>60% G, 75–220 kDa MW, NovaMatrix, Sandvika, Norway) was dissolved at 1.4% weight to volume in 0.8% saline. SLG100 (>60% G, 200–300 kDa MW, NovaMatrix, Sandvika, Norway) was dissolved at 1.2% weight to volume in 0.8% saline. UPVLVG (NovaMatrix, Sandvika, Norway) was dissolved at 5% weight to volume in 0.8% saline. All modified alginates were initially dissolved at 5% weight to volume in 0.8% saline. Modified alginates were then blended with 3% weight to volume SLG100, dissolved in 0.8% saline. Blend ratios for each formulation were determined

empirically (% volume modified alginate/% volume SLG100): Z2-Y12 (70/30), N8 (80/20), O6 (60/40), O9 (60/40), O11 (50/50), O3 (80/20), Z1-Y15 (80/20), Z1-Y2 (50/50), Z1-Y19 (70/30), N7 (80/20), VLVG/SLG100 (V/S, 80/20). For Z2-Y12, the addition of 0.01% detergent (Tween 20) to the gelation bath sometimes proved helpful for sphere formation.

For formation of 300–350 μm diameter microcapsules, a 30-gauge blunt-tipped needle (SAI Infusion Technologies) was used with a voltage of 7–8 kV. For formation of 1.35–1.5 mm spheres, an 18-gauge blunt tipped needle (SAI Infusion Technologies) was used with a voltage of 5–7 kV.

Implantation of the hydrogel microcapsules and spheres

All animal protocols were approved by Animal Care Committees at both MIT and UIC (for primate studies), and all surgical procedures and post-operative care was supervised by MIT Division of Comparative Medicine veterinary staff. After implantation, mice were randomized by number assignment to blind investigators. Samples obtained for analysis were unblinded only after implantation outcome was assessed. Immune-competent male C57BL/6J mice (Jackson Laboratory, Bar Harbor, ME) were anesthetized with 3% isoflurane in oxygen and had their abdomens shaved and sterilized using betadine and isopropanol. A 0.5 mm incision was made along the midline of the abdomen and the peritoneal lining was exposed using blunt dissection. The peritoneal wall was then grasped with forceps and a 0.5–1 mm incision was made along the linea alba. A volume of 350 μl of microcapsules was then loaded into a sterile pipette and implanted into the peritoneal cavity through the incision. The incision was then closed using 5–0 taper tipped polydioxanone (PDS II) absorbable sutures. The skin was then closed over the incision using a wound clip and tissue glue. Preoperatively, all mice also received a 0.05 mg/kg dose of buprenorphine subcutaneously as a pre-surgical analgesic, along with 0.3 ml of 0.9% saline subcutaneously to prevent dehydration.

Non-human primate implantations were performed following the procedure outlined in Qi, M. *et al*.[49]. Briefly, the animal was fasted for 12 h before surgery. Prior to surgery, the animal was given buprenorphine (0.01–0.03 mg/kg) as a pre-operative analgesic, and cefazolin (25 mg/kg) as a prophylactic antibiotic, via intramuscular injection. The animal was then sedated with ketamine (10 mg/kg) given intravenously as an induction agent. Intubation and a continuous infusion of isofluorane gas through an endotracheal tube was maintained through the duration of the procedure.

The animal was placed in a supine position and the abdomen shaved and sterilized using alternating scrubs of betadine and isopropyl alcohol. The animal was be moved to the operating surface and the maintenance of body temperature aided by the use of a heated, circulating water pad. A sterile area was established with the use of surgical drapes. A small 2 cm supra-umbilical incision was made and a 5 mm trocar was positioned. A pneumoperitoneum was established using a commercial insufflator and CO_2 with the pressure maintained at 12 mm Hg. A second 1–2 cm incision was made along the midline and a second 5 mm trocar was positioned. A non-heat generating light source and video laparoscope was inserted through one trocar and images of the abdominal viscera were taken to assure normalcy. A sterile, flexible catheter was inserted through the second trocar and

used to distribute the capsules throughout the abdominal cavity. The implant of 10 ml of hydrogel capsules were suspended in 30 ml of 0.9% sterile saline and gently infused at a rate no greater than 30 ml/min. The abdomen was then desufflated and the trocars were removed. The small incisions created by the trocars were then closed using a simple, interrupted pattern using an absorbable suture and tissue glue.

Retrieval of cells, tissues and materials

At desired time points post-implantation, as specified in figures, mice were euthanized by CO_2 administration, followed by cervical dislocation. In certain instances, 5 ml of ice cold PBS was first injected in order perform an intraperitoneal lavage to rinse out and collect free-floating intraperitoneal immune cells. An incision was then made using the forceps and scissors along the abdomen skin and peritoneal wall, and intraperitoneal lavage volumes were pipetted out into fresh 15 ml falcon tubes (each prepared with 5 ml of RPMI cell culture media). Next, a wash bottle tip was inserted into the abdominal cavity. KREBS buffer was then used to wash out all material capsules from the abdomen and into Petri dishes for collection. After ensuring all the capsules were washed out or manually retrieved, if fibrosed directly to intraperitoneal tissues, they were transferred into 50 ml conical tubes for downstream processing and imaging. Using this method, we recover 70% of the original implant volume, about 250 μl of capsules. In the case of Z2-Y12, after intraperitoneal lavage and capsule retrieval intraperitoneal fat pad tissue was also excised for downstream FACS and expression analyses.

Non-human primate retrievals were performed at the specified time points following the procedure outlined in Qi, M. *et al.*[2]. Survival retrieval surgeries were conducted using the same methods described for implantation, with the exception that capsules were retrieved instead of implanted. Approximately 30 ml of sterile 0.9% saline was used to gently flush the peritoneal cavity and then gently aspirated back into the syringe. Closure was conducted with the same methods described for implantation. The level of adhesions and bioreactivity were also assessed. Images of the abdominal viscera and the positioning of the capsules were taken. Samples of the omentum were also be taken to test for embedded capsules and fibrosis. Throughout, clinical health was monitored by veterinary staff.

Imaging of the retrieved material capsules

For phase contrast imaging retrieved materials were gently washed using Krebs buffer and transferred into 35 mm Petri dishes for dark-field microscopy using an Evos Xl microscope (Life Technologies).

Subcutaneous cathepsin measurement of implanted capsules

Female SKH1 mice (6 weeks old) were used for this assay. A volume of 100 μl of capsules were resuspended in 200 μl of saline, and injected subcutaneously into the mouse on the left side of upper back. The mice were fed on AIN-93G purified rodent diet (TD 94045, Harlan) to minimize the fluorescent background after injection. Six days later, 100 μl (4 nmol) of ProSense 750 FAST (NEV11171, PerkinElmer Inc.) per mouse was injected intravenously via tail vein. At day 7 (i.e., 24 h post the ProSense 750 FAST intravenous administration), the mice were scanned by IVIS Spectrum system (Xenogen, Caliper LifeScience). The mice

were anesthetized using 3% isofluorane in oxygen and maintained at the same rate throughout the procedure, and the settings of the IVIS Spectrum system were Exposure = 7.50, Binning = Medium, FStop = 2, Excitation = 605 and Emission = 660. The images were analyzed with Living Image Software, and the right side of upper back on the same mouse was used as a background control for signal quantification.

In vitro cathepsin activity assay

Recombinant Mouse Cathepsin B (rmCathepsin B, R&D system, 965-CY-010) was diluted to 10 μM in Activation Buffer (25 mM MES, 5 mM DTT, pH 5.0), incubated at room temperature for 15 min (activation step). Then the activated rmCathepsin B was diluted in Assay Buffer (25 mM MES, pH 5.0) and transferred into the wells of a 96-well plate, the final concentration was 0.1 μM. The substrate (Prosense 750 Fast, PerkinElmer, NEV11171) and barium chloride (A Johnson Matthey Company, A12905) was diluted in assay buffer and transferred into the wells which contained the rmCathepsin B, the final concentration of the substrate was 0.5 μM and barium chloride was 20 mM. Substrate blank and rmCathepsin B blank were included as controls. Fluorescence measurements were then recorded after a 2 h incubation at room temperature using excitation and emission wavelengths of 750 nm and 780 nm.

Recombinant Mouse Cathepsin L (rmCathepsin L, R&D system, 1515-CY-010) was diluted to 10 μM in activation buffer (25 mM NaOAc, 5 mM dithiothreitol (DTT), pH 5.0), incubated at room temperature for 16–20 h (overnight). The activated rmCathepsin L was diluted in assay buffer (25 mM MES, 5 mM DTT, pH 6.0) and transferred into the wells of a 96-well plate, with a final concentration of 0.1 μM. The substrate (Prosense 750 Fast, PerkinElmer, NEV11171) and barium chloride (A Johnson Matthey Company, A12905) was diluted in assay buffer and transferred into the wells which contained the rmCathepsin L, the final concentration of the substrate was 0.5 μM and barium chloride was 2 0 mM. A substrate blank and rmCathepsin B blank were included as controls. Fluorescence measurements were then recorded after a 2 h incubation at room temperature using excitation and emission wavelengths of 750 nm and 780 nm.

Subcutaneous histology

At 28 d after subcutaneous implantation, mice were euthanized by CO_2 asphyxiation. The implanted capsules and surrounding tissue, including the skin, of approximately 2 cm in diameter were dissected and placed into tissue prep cassettes appropriate to the size of the samples. They were then fixed in 10% formalin (NBF-4-G, Azer Scientific) for 24 h. The fixed tissues were embedded in paraffin and cut into 5 μm sections and processed in The Hope Babette Tang Histology Facility in Koch Institute of MIT. Finally, section were stained with Hematoxylin and Eosin (H&E) staining and Masson's Trichrome (MT) staining using standard methods.

Histology quantification

Data were collected from sectioned tissue within 51 μm from the tissue-implant interface in Masson's trichrome stained slides. Five different fields were randomly examined in each section, and three sections were analyzed, with each section coming from a different

biological replicate. Blue pixel density was measured in MATLAB as a function of distance from the tissue-implant interface, and expressed as a percentage of average maximum pixel density as determined from all analyzed sections. All data are presented as the mean of all measurements.

PCA analysis

The chemical functional groups of all modifications in the alginate library were identified manually. Principal components analysis (PCA) was performed on the number of various types of functional groups, and the library was plotted along the first two principal components using the software package R. The top performing modifications were indicated upon processing.

Cell staining and confocal immunofluorescence

Retrieved samples were fixed in 4% paraformaldehyde overnight (diluted in 1× PBS). Samples were then washed in Krebs Buffer (7.889 g NaCl, 0.35 g KCl, 5.958g HEPES (Sigma-Aldrich, Montana, USA), 0.163 g KH_2PO_4, 0.144g $MGSO_4$ * $7H_2O$ in 1,000 ml of DiH_2O). Samples were washed with PBS three times. PBS was aspirated and a 1% Triton X-100 (Sigma-Aldrich, Montana, USA) solution was used to permeabilize cells. Samples were incubated for 10 min at room temperature. Samples were then incubated with 1% albumin solution (Sigma-Aldrich, Montana, USA), diluted in 1× PBS for 30 min at room temperature. 3 ml of antibody solution (1:200 CD68 488 Anti-Mouse (CA#137012, BioLegend California, USA)[35], 1:200 Anti-Mouse Actin, α-Smooth Muscle-Cy3 (CA# C6198, Sigma-Aldrich, Montana, USA)[35], 1:200 anti-mouse CD68-AF488 (BioLegend), and DAPI (NucBlue Live Cell Stain ReadyProbes, Life Technologies, California, USA) 2 drops per ml) all diluted in 1% albumin solution was added to each sample. Samples were incubated in staining solution for 45 min at room temperature. Staining solution was then aspirated. Samples were then washed twice with 0.1% tween 20 solution (Sigma-Aldrich, Montana, USA), diluted in 1× PBS. Samples were then washed twice with 1× PBS. Samples were then transferred to a 24-well glass bottom plate. Excess PBS was aspirated and 1 ml of 50% glycerol solution (Sigma-Aldrich, Montana, USA) was added. A Zeiss LSM 700 system with ZEN microscope software was used to image and analyze the stained samples. Obtained images where adjusted linearly for presentation using Photoshop (Adobe Inc. Seattle, WA).

Protein extraction

Retrieved capsules were sonicated with three 30 s pulses at 70% amplitude (QSonica Sonicator, Model#Q125, QSonica LLC) on ice using either RIPA buffer (Pierce, cat. #89901, ThermoScientific) for western blot analysis or NP40 cell lysis buffer (cat #FNN0021, Invitrogen) for Elispot analysis. A ratio of 100 μl capsules to 200 μl lysis buffer with 100 mM PMSF and 1× protease inhibitors (Halt Protease inhibitor single-use cocktail, Cat. #78430, Thermo Scientific). Lysates were centrifuged for 20 min at 12,000 r.p.m. at 4 °C, the supernatant which contains proteins was aspirated into a fresh tube kept on ice. The pellets were washed with the same volume of lysis buffer (i.e., the pellet of 100 μl capsules were washed with 200 μl lysis buffer), and then centrifuged for 20 min at 12,000

r.p.m. at 4 °C, combined the supernatant with the previous one. The proteins were stored at –80 °C for future use.

Mouse cytokine array

This assay was accomplished with Proteome Profiler Mouse Cytokine Array Panel A kit (Cat#ARY006, R&D system)[35]. For each membrane, 200 μl of protein solution was mixed with 100 μl of sample buffer (array buffer 4) and 1.2 ml of block buffer (array buffer 6), then added with 15 μl of reconstituted Mouse Cytokine Array Panel A Detection Antibody Cocktail and incubated at room temperature for 1 h. The array membrane was incubated with block buffer (array buffer 6) for 2 h on a rocking platform shaker in the meantime, and then the block buffer was aspirated, the prepared sample/antibody mixture was added onto the membrane and incubated overnight at 4 °C on a rocking platform shaker. The membrane was washed with 20 ml of 1× wash buffer for 10 min on a rocking platform shaker for three time and rinsed with deionized water once, then was probed with Fluorophore-conjugated streptavidin (1:5,000 dilution, Cat#926-32230, Li-Cor) at room temperature for 30 min on a rocking platform shaker, washed with wash buffer for three times and rinsed with deionized water once again as in above steps. Antibody-antigen complexes were visualized using Odyssey Detection (Li-Cor, Serial No. ODY-2329) at 800 nm wavelengths. The densities of the spots were analyzed by Image J software.

Western blot analysis

A volume of 12 μl of protein solution (see Protein Extraction) was mixed with 1× loading buffer (SDS-Sample buffer, Cat.#BP-111R, Boston BioProducts) for each lane, boiled at 95 °C for 20 min, and electrophoresed on SDS polyacrylamide gels (Any K_d 15-well comb mini-gel, Bio-Rad, Cat # 456-9036). A volume of 3 μl of Precision Plus Protein Dual Xtra Stands (Cat#161-0377, Bio-Rad) was used as ladder to indicate the position of the bands, and then blotted onto nitrocellulose membranes (Biorad, Cat. # 162-0213). Blots were probed with anti-αSmooth Muscle actin antibody (1:400 dilution, Rabbit polyclonal to alpha smooth muscle Actin; Cat. # ab5694, AbCam) and anti-P actin antibody (1:4,000 dilution, Monoclonal Anti-β-Actin antibody produced in mouse; Cat #A1978, Sigma Aldrich) as a loading control followed by Donkey Anti-Rabbit (1 to 15,000 dilution, Cat#926-32213, Li-Cor) and Goat Anti-Mouse(1 to 15,000 dilution, Cat#926-68070, Li-Cor) Fluorophore-conjugated secondary antibodies. Antibody-antigen complexes were visualized using an Odyssey Detection system (Li-Cor, Serial No. ODY-2329) at 700 and 800 nm wavelengths. The densities of the bands were analyzed by Image J software.

Hydroxyproline assay (collagen content)

Protein from 100 μl of retrieved capsules (mice or non-human primates) were extracted with RIPA buffer and concentrations were quantified by BCA assay as described in the Protein Extraction section. All samples and standards were run in duplicate. RIPA buffer was used for the preparation of standards and samples. To quantify collagen content, a hydroxyproline quantification kit (Sigma-Aldrich MAK008-1KT) was used and run according to manufacturer's instructions. Briefly, a standard curve was prepared each time the assay was run by preparing hydroxyproline standards for colorimetric detection. A volume of 10 μl of the 1 mg/ml Hydroxyproline Standard Solution was diluted with 1.99 ml of water to prepare

a 0.005 mg/ml standard solution. 0, 1.5, 3, 6, 12, 25, 50 and 100 µl of the 0.005 mg/ml hydroxyproline standard solution were added into a 96 well plate, generating 0 (blank), 0.0075, 0.015, 0.03, 0.06, 0.125, 0.25 and 0.5 µg/well standards. A quantity of 20 µg of protein of each sample prepared above was transferred to a 2.0 ml polypropylene tube, diluted with water up to 100 µl. 100 µl of concentrated hydrochloric acid (HCl, ∼12 M) was added, capped tightly, wrapped with parafilm and aluminum foil, and hydrolyzed at 120 °C for 3 h. The supernatant was transferred to a 96 well plate. Then all wells were evaporated to dryness in a 60 °C oven overnight. A volume of 100 µl of the Chloramine T/Oxidation Buffer (6 µl of Chloramine T Concentrate to 94 µl of Oxidation Buffer) was then added and mixed to each protein sample and standard well and incubated at room temperature for 5 min. A volume of 100 µl of the diluted DMAB reagent (50 µl of DMAB Concentrate to 50 µl of perchloric acid/isopropanol solution) was added and mixed to each protein sample and standard well, and incubated at 60 °C for 90 min. The absorbance at 560 nm (A560) was measured. The value obtained from the 0 (blank) hydroxyproline standard was the background for the assay, which was subtracted from all readings. The values obtained from the appropriate hydroxyproline standards were used to plot a standard curve. The amount of hydroxyproline present in the samples was then determined from the standard curve.

CellTiter glo assay (cell viability assay)

RAW 264.7 cells were plated (CA#TIB-71, ATCC, VA, USA, identified by manufacturer and mycoplasma tested) at a density of 100,000 cells per well in a 96 well Culture Plate (Cellstar, MA, USA). The culture media used was DMEM (High Glucose, GlutaMAX, L-Glutamine, Phenol Red) with 10% HiFBS and 1% Penicillin Streptomycin (Life Technologies, MA, USA). 24 h later, 100 µl of 0.5 mm alginate beads were plated on top of the cells in each well of the plate; these alginate beads were prepared as previously described. These alginate beads were transferred to culture media and then added to the plated cells and incubated for 24 h at 37 °C in a cell culture incubator. The alginate bead treatments were SLG20 at 1.4% in saline, UPVLVG blended with SLG100 at 5% and 3% in saline respectively (80:20), Z1-Y15 blended with SLG100 at 5% and 3% in saline respectively (80:20), Z1-Y19 blended with SLG100 at 5% and 3% in saline, respectively (70:30), and Z2-Y12 blended with SLG100 at 5% and 3% in saline, respectively (70:30). Cells were plated alone with no beads as a control. 24 h after the alginate beads added, the CellTiter-Glo Luminescent Viability assay was done (Promega, WI, USA). The treated culture plate was left at room temperature for 30 min and then 100 µl of the CellTiter-Glo substrate (G755A) was then added to each well. The plate with cells, alginate, and substrate was mixed at 300 rpm for 2 min to lyse the cells, then left at room temperature to equilibrate for 10 min. Finally, 100 µl of the mixture was transferred to a flat bottom, white, 96 well plate (Costar, MA, USA) and read with a luminescent plate reader (Infinite M200 Pro, Tecan, NC).

Protein adsorption

Solutions of 5% (w/v) modified alginates (Z1-Y19, Z1-Y15 and Z2-Y12) and UPVLVG alginate in 0.8% saline were mixed with a 3% SLG100 solution in 0.8% saline, respectively, at the ratio of 70:30. A solution of 1.4% SLG20 was prepared separately and was not mixed. A volume of 100 µl of the SLG20 solution and the above mixtures were added to each well

of a 96-well plate and 100 μl of cross-linking buffer (20 mM barium chloride) was added on the top of the gel. After brief centrifugation, the plate was kept still for 1 h for solidification. Each well was washed with PBS once, 100 μl of PBS diluted Fetal Bovine Serum solution (final concentration was 1.5 mg/ml) were added and incubated for 4 h at room temperature. The liquid in each well was aspirated carefully and washed with PBS three times. The gel was taken out and sonicated as described in the Protein Extraction Procedure, the protein released from the gel was measured by BCA assay (Pierce BCA Protein Assay kit, Cat # 23225, Thermo Scientific).

Endotoxin and glucan testing

All endotoxin and glucan testing was performed by Charles River Laboratories. Sterile microcapsules of 300–350 μm diameters for Z2-Y12, Z1-Y15, Z1-Y19, V/S, SLG20, and commercial non-ultrapure alginate from Sigma Aldrich #W201502 were prepared as described in **Microcapsule/sphere formation**. In addition, microcapsules from a commercial non-ultrapure alginate from Sigma Aldrich #W201502 were prepared and submitted as a positive control. Microcapsules were suspended in sterile, endotoxin-free 0.8% saline solution and submitted to Charles River Laboratories, where the Limulus amoebocyte lysate (LAL) test was implemented using the kinetic Endosafe Portable Test System (PTS). A volume of 1 ml of microcapsules were loaded into cartridges for testing and endotoxin-free saline was used as a negative control.

General lipoteichoic acid ELISA

A volume of 100 μl of microcapsules from each material group (SLG20, V/S, Z1-Y19, Z1-Y15 and Z2-Y12, and commercial non-ultrapure alginate from Sigma Aldrich #W201502) was sonicated and homogenized as described in 20 ml of pure, endotoxin-free deionized water. Once the capsules had completely dissolved, the solution was lyophilized and then reconstituted in 100 μl of assay buffer. Human Lipoteichoic acid ELISA kit (MyBiosource Catalog #MBS268197) was used in this assay, which has a manufacturer's reported detection range of 0.312 to 20 ng/ml. All reagents were equilibrated to room temperature, working standards were prepared from 10.0 ng/ml through 0.312 ng/ml, and the standard sample diluent was served as the 0 standard, as described in the manufacturer's instructions. A volume of 100 μl of standard, blank, or sample were added per well, sealed and hatched in incubator at 37 °C for 90 min. Six replicates were run for each sample tested. Each well was aspirated and washed with washing buffer three times. A volume of 100 μl of biotinylated LTA antibody liquid were added to each well immediately, the plate was sealed and incubated for 1 h at 37 °C. Each well was aspirated and washed with washing buffer three times. A volume of 100 μl of enzyme-conjugate liquid were added to each well, sealed and incubated for 30 min at 37 °C. Each well was aspirated and washed with washing buffer five times. 100 μl of color reagent liquid were added to each well, sealed and incubated for 15–30 min at 37 °C, protected from light. Finally, 100 μl of color reagent C were added to each well, then the optical density of each well was determined at 450 nm, with the optical density at 630 nm serving as a correction wavelength.

Mouse flagellin ELISA

A volume of 250 μl of microcapsules from each material group (SLG20, V/S, Z1-Y19, Z1-Y15, Z2-Y12, and a commercial non-ultrapure alginate from Sigma Aldrich #W201502) was sonicated and homogenized as described in 20 ml of pure, endotoxin-free deionized water. Once the capsules had completely dissolved, the solution was lyophilized and then reconstituted in 100 μl of assay buffer. Mouse Flagellin ELISA kit (MBS267926, MyBioSource) was used in this assay, which has a manufacturer's reported detection range of 78–5000 pg/ml. All reagents were equilibrated to room temperature, working standards were prepared from 1,250 pg/ml through 78 pg/ml, and the diluent was served as the 0 standard. 100 μl of Standard, Blank, or Sample were added per well, the plated was sealed and incubated for 90 min at 37 °C. Five replicates were run for each sample tested. Each well was aspirated and washed with washing buffer three times. 100 μl of the biotinylated Mouse Flagellin antibody liquid were added to each well, sealed and incubated for 60 min at 37 °C. Each well was aspirated and washed with washing buffer three times. A volume of 100 μl of enzyme-conjugated liquid were added to each well, sealed and incubated for 30 min at 37 °C. Each well was aspirated and washed with washing buffer five times, and then 100 μl of Color Reagent liquid were added to each well, sealed and incubated at 37 °C no more than 30 min until darker color for high concentration of standard curve and color gradient were observed. Finally, 100 μl of Color Reagent C was added to each well to stop the reaction and the plate was read at 450 nm within 10 min.

Mechanical testing and Young's modulus determination

Mechanical parallel plate compression measurements were performed by CellScale Biomaterials Testing using a CellScale MicroSquisher. Spheres from each material group from each material group (SLG20, V/S, Z1-Y19, Z1-Y15 and Z2-Y12) were compressed between a fixed stainless steel block and a moving stainless steel upper platen. The samples were immersed in room temperature saline solution (Fisher Scientific 312651) for testing. The samples were transferred to the testing chamber using a pipette. The diameter of each sample was determined using the control software measuring tool and then each sample was compressed by 40% of its initial diameter in 80s and unloaded in 80s. Five or more samples of each specimen type were tested. Images and data (time, force, displacement, and size) were collected at 1 Hz for the duration of the test. Young's modulus for each sample was then determined as described in Kim *et al.*[47].

Profilometry

Surface profiling and roughness measurements were performed with a Bruker Dektak XT stylus profilometer. A volume of 100 μl of 1.35–1.5 mm diameter spheres were placed on a glass microscope slide, with excess solution wicked off using a kimwipe. Three spheres from each material group (SLG20, V/S, Z2-Y12, Z1-Y15 and Z1-Y19) were profiled using a standard scan with a hills and valley profile and a 6.5 μm range over a 300 μm distance for 15 s. The stylus used had a radius of 12.5 μm and a stylus force of 2 mg was applied. Surface roughness (P_a) was determined from each profile using the Vision64 software.

NanoString analysis

RNAs for mock-implanted (MT) controls, or 300 μm alginate capsule-bearing mice (n = 5/group) were isolated from tissue samples taken at various time points after implantation. RNAs were quantified, diluted to the appropriate concentration (100 ng/μl), and 500 ng of each sample was processed according to NanoString manufacturer protocols for expression analysis via our customized multiplexed 79-gene inflammation and immune cell marker panel. RNA levels (absolute copy numbers) were obtained following nCounter (NanoString Technologies Inc., Seattle, WA) quantification, and group samples were analyzed using nSolver analysis software (NanoString Technologies Inc., Seattle, WA).

FACS analysis

Single-cell suspensions of freshly excised tissues were prepared using a gentleMACS Dissociator (Miltenyi Biotec, Auburn, CA) according to the manufacturer's protocol. Single-cell suspensions were prepared in PEB dissociation buffer (1× PBS, pH 7.2, 0.5% BSA, and 2 mM EDTA) and suspensions were passed through 70 μm filters (Cat. #22363548, Fisher Scientific, Pittsburgh, PA). All tissue and material sample-derived, single-cell populations were then subjected to red blood cell lysis with 5 ml of 1× RBC lysis buffer (Cat. #00-4333, eBioscience, San Diego, CA, USA) for 5 min at 4 °C. The reaction was terminated by the addition of 20 ml of sterile 1× PBS. The cells remaining were centrifuged at 300–400g at 4 °C and resuspended in a minimal volume (~50 μl) of eBioscience Staining Buffer (cat. #00-4222) for antibody incubation. All samples were then co-stained in the dark for 25 min at 4 °C with two of the fluorescently tagged monoclonal antibodies specific for the cell markers CD68 (1 μl (0.5 μg) per sample; CD68-Alexa647, Clone FA-11, Cat. #11-5931, BioLegend)[35], Ly-6G (Gr-1) (1 μl (0.5 μg) per sample; Ly-6G-Alexa-647, Clone RB6-8C5, Cat. #108418, BioLegend)[35], CD11b (1 μl (0.2 μg) per sample; or CD11b-Alexa-488, Clone M1/70, Cat. #101217, BioLegend)[35].

Two ml of eBioscience Flow Cytometry Staining Buffer (cat. #00-4222, eBioscience) was then added, and the samples were centrifuged at 400–500 g for 5 min at 4 °C. Supernatants were removed by aspiration, and this wash step was repeated two more times with staining buffer. Following the third wash, each sample was resuspended in 500 μl of Flow Cytometry Staining Buffer and run through a 40 μm filter (Cat. #22363547, Fisher Scientific) for eventual FACS analysis using a BD FACSCalibur (cat. #342975), BD Biosciences, San Jose, CA, USA). For proper background and laser intensity settings, unstained, single antibody, and IgG (labeled with either Alexa-488 (CA# 400625)[35] or Alexa-647 (CA# 400526, BioLegend)[35] controls were also run.

Intravital imaging

For intravital imaging, 300 μm SLG20 and Z2-Y12 hydrogel capsules were loaded with Qdot 605 (Life technologies, Grand Island, NY) and surgically implanted into C57BL/6J-Tg(Csf1r-EGFP-NGFR/FKBP1A/ TNFRSF6)2Bck/J mice (MAFIA) as described above. After 7 d post implantation, the mice were placed under isoflurane anesthesia and a small incision was made at the site of the original surgery to expose beads. The mice were placed on an inverted microscope and imaged using a 25×, N.A. 1.05 objective on an Olympus FVB-1000 MP multiphoton microscope at an excitation wavelength of 860 nm. Z-stacks of

200 μm (10 μm steps) were acquired at 2-min intervals for time series of 20–45 min depending on the image. The mice were kept under constant isoflurane anesthesia and monitored throughout the imaging session. Obtained images were analyzed using Velocity 3D Image Analysis Software (Perkin Elmer, Waltham, MA).

Confocal Raman spectroscopy

Sample preparation—A drop of hydrogel capsules with buffer solution was dried on the quartz coverslip (043210-KJ, Alfa Aesar). In order to remove the salt from the dried buffer solution, a drop of distilled water was gently applied on top of the dried sample and immediately absorbed by a tissue. This preparation was critical for Raman mapping of the dried hydrogel capsules.

Instrumentation—A custom-built near-infrared confocal Raman microscopy system was previously reported[55,56]. Briefly, a 785 nm wavelength Ti: Sapphire laser (3900S, Spectra-Physics) was used for sample excitation. The collimated beam was filtered by a band pass filter (BPF, LL01-785-12.5, Semrock) and redirected to the dual axes galvanometer mirrors. High-speed XY scanning was performed by the galvanometer mirrors (CT-6210, Cambridge Technology). A 1.2 NA water immersion objective lens (Olympus UPLSAPO60XWIR 60X/1.20) was used to both focus the laser light onto the sample and to collect the back-scattered light. A piezo actuator combined with a differential micrometer (DRV517, Thorlabs) was used to perform the coarse and fine adjustments, respectively, of the sample focus. A flip mirror was placed after the tube lens so that the sample focal plane from the incoherent transmission source can be observed using a video camera with 75× magnification. The back-scattered Raman light from the sample passes through two dichroic mirrors (DM1: Semrock LPD01-785RU-25, DM2: Semrock LPD01-785RU-25×36×1.1) and was collected by a multi-mode fiber (Thorlabs M14L01). The collected signal was delivered to the spectrograph (Holospec f/1.8i, Kaiser Optical Systems) and detected by a thermoelectric-cooled, back-illuminated and deep depleted CCD (PIXIS: 100BR_eXcelon, Princeton Instruments). LabView 8.6 software (National Instruments), data acquisition board (PCI-6251, National Instruments) and MATLAB 2013 software (Mathworks) were used to control the system, acquire the data, and analyze the data.

Raman spectroscopy measurement—60 mW of 785 nm laser power was focused to a micrometer spot size and used to raster scan the hydrogel samples. 30 × 30 spectra were acquired from 45 μm × 45 μm area with an integration time 1.0 s/pixel. The total measurement time was approximately 15 min.

Data processing—Two Raman images are generated based on the intensities of two Raman bands (for Z2-Y12: 830 cm^{-1} and 1,000 cm^{-1}, for Z1-Y15: 857 cm^{-1} and 884 cm^{-1}, for Z1-Y19: 1563 cm^{-1} and 884 cm^{-1}) These Raman images are resized and overlaid as red and green colors on top of corresponding bright-field image from the same area.

Cryo-SEM sample preparation and imaging

Cryo-SEM images of 300 μm microcapsules where acquired using a Zeiss NVision 40 (Carl Zeiss SMT, Inc.) field emission scanning electron microscope at an acceleration voltages of

1–2 kV. To prepare samples for imaging approximately 100 μl of microcapsules where transferred to a sample stub and then plunged into a slushy liquid and solid nitrogen bath. The samples where next transferred to an EM VCT100 vacuum cryo transfer system (Leica Microsystems, Inc.) to selectively remove surface water (ice) by controlled specimen sublimation. The frozen sample where then further fractured with a sharp blade and sputter coated with a thin layer of platinum and palladium metals before imaging.

Supplementary Material

Refer to Web version on PubMed Central for supplementary material.

Acknowledgments

This work was supported jointly by the JDRF and Leona M. and the Harry B. Helmsley Charitable Trust (grant 3-SRA-2014-285-M-R), National Institutes of Health (NIH grants EB000244, EB000351, DE013023 and CA151884), NIH NIBIB (P41EB015871-27), MIT SkolTech initiative (J.W.K.), JDRF and the Department of Defense/Congressionally Directed Medical Research Programs (DOD/CDMRP postdoctoral fellowships 3-2013-178 and W81XWH-13-1-0215 for O.V.) and through a generous gift from the Tayebati Family Foundation. G.C.W. is supported by National Institutes of Health (NIH grants R01DK093909 and P30DK036836, the Joslin Diabetes Research Center and its Advanced Microscopy Core), as well as the Diabetes Research and Wellness Foundation. J.O. is supported by the National Institutes of Health (NIH/NIDDK) R01DK091526 and the Chicago Diabetes Project. This work was also supported in part by the Koch Institute Support (core) grant P30-CA14051 from the National Cancer Institute. We also thank the Koch Institute Swanson Biotechnology Center for technical support, specifically Tang Histology Facility, Microscopy, Flow Cytometry, Nanotechnology Materials, and Applied Therapeutics and Whole Animal Imaging. The authors would like to acknowledge the use of resources at the Harvard University Center for Nanoscale Systems and W.M. Keck Biological Imaging Facility (Whitehead Institute). The authors would also like to thank W. Salmon and J. Wyckoff for their assistance.

References

1. Anderson JM, Rodriguez A, Chang DT. Foreign body reaction to biomaterials. Semin. Immunol. 2008; 20:86–100. [PubMed: 18162407]
2. Langer R. Perspectives and challenges in tissue engineering and regenerative medicine. Adv. Mater. 2009; 21:3235–3236. [PubMed: 20882493]
3. Ward WK. A review of the foreign-body response to subcutaneously-implanted devices: the role of macrophages and cytokines in biofouling and fbrosis. J. Diabetes Sci. Technol. 2008; 2:768–777. [PubMed: 19885259]
4. Harding JL, Reynolds MM. Combating medical device fouling. Trends Biotechnol. 2014; 32:140–146. [PubMed: 24438709]
5. Grainger DW. All charged up about implanted biomaterials. Nat. Biotechnol. 2013; 31:507–509. [PubMed: 23752436]
6. Williams DF. On the mechanisms of biocompatibility. Biomaterials. 2008; 29:2941–2953. [PubMed: 18440630]
7. Wick G, et al. The immunology of fbrosis. Annu. Rev. Immunol. 2013; 31:107–135. [PubMed: 23516981]
8. Wynn TA, Ramalingam TR. Mechanisms of fbrosis: therapeutic translation for fbrotic disease. Nat. Med. 2012; 18:1028–1040. [PubMed: 22772564]
9. Zhang L, et al. Zwitterionic hydrogels implanted in mice resist the foreign-body reaction. Nat. Biotechnol. 2013; 31:553–556. [PubMed: 23666011]
10. Sussman EM, Halpin MC, Muster J, Moon RT, Ratner BD. Porous implants modulate healing and induce shifts in local macrophage polarization in the foreign body reaction. Ann. Biomed. Eng. 2013; 42:1508–1516. [PubMed: 24248559]
11. Rodriguez A, Meyerson H, Anderson JM. Quantitative *in vivo* cytokine analysis at synthetic biomaterial implant sites. J. Biomed. Mater. Res. A. 2009; 89:152–159. [PubMed: 18431759]

12. Hetrick EM, Prichard HL, Klitzman B, Schoenfsch MH. Reduced foreign body response at nitric oxide-releasing subcutaneous implants. Biomaterials. 2007; 28:4571–4580. [PubMed: 17681598]
13. Ratner BD. Reducing capsular thickness and enhancing angiogenesis around implant drug release systems. J. Control. Release. 2002; 78:211–218. [PubMed: 11772462]
14. Lee KY, Mooney DJ. Alginate: properties and biomedical applications. Prog. Polym. Sci. 2012; 37:106–126. [PubMed: 22125349]
15. Kearney CJ, Mooney DJ. Macroscale delivery systems for molecular and cellular payloads. Nat. Mater. 2013; 12:1004–1017. [PubMed: 24150418]
16. Lim F, Sun AM. Microencapsulated islets as bioartifcial endocrine pancreas. Science. 1980; 210:908–910. [PubMed: 6776628]
17. Duvivier-Kali VF, Omer A, Parent RJ, O'Neil JJ, Weir GC. Complete protection of islets against allorejection and autoimmunity by a simple barium-alginate membrane. Diabetes. 2001; 50:1698–1705. [PubMed: 11473027]
18. de Vos P, Faas MM, Strand B, Calafore R. Alginate-based microcapsules for immunoisolation of pancreatic islets. Biomaterials. 2006; 27:5603–5617. [PubMed: 16879864]
19. Tuch BE, et al. Safety and viability of microencapsulated human islets transplanted into diabetic humans. Diabetes Care. 2009; 32:1887–1889. [PubMed: 19549731]
20. Weir GC. Islet encapsulation: advances and obstacles. Diabetologia. 2013; 56:1458–1461. [PubMed: 23636639]
21. Jacobs-Tulleneers-Thevissen D, et al. Beta Cell Therapy Consortium EU-FP7. Sustained function of alginate-encapsulated human islet cell implants in the peritoneal cavity of mice leading to a pilot study in a type 1 diabetic patient. Diabetologia. 2013; 56:1605–1614. [PubMed: 23620058]
22. Scharp DW, Marchetti P. Encapsulated islets for diabetes therapy: history, current progress, and critical issues requiring solution. Adv. Drug Deliv. Rev. 2014; 67–68:35–73.
23. Robitaille R, et al. Infammatory response to peritoneal implantation of alginate-poly-l-lysine microcapsules. Biomaterials. 2005; 26:4119–4127. [PubMed: 15664639]
24. Dang TT, et al. Enhanced function of immuno-isolated islets in diabetes therapy by co-encapsulation with an anti-infammatory drug. Biomaterials. 2013; 34:5792–5801. [PubMed: 23660251]
25. Rokstad AM, et al. Alginate microbeads are complement compatible, in contrast to polycation containing microcapsules, as revealed in a human whole blood model. Acta Biomater. 2011; 7:2566–2578. [PubMed: 21402181]
26. King A, Sandler S, Andersson A. The effect of host factors and capsule composition on the cellular overgrowth on implanted alginate capsules. J. Biomed. Mater. Res. 2001; 57:374–383. [PubMed: 11523032]
27. Manoury B, Caulet-Maugendre S, Guénon I, Lagente V, Boichot E. TIMP-1 is a key factor of fbrogenic response to bleomycin in mouse lung. Int. J. Immunopathol. Pharmacol. 2006; 19:471–487. [PubMed: 17026855]
28. Brocchini S, James K, Tangpasuthadol V, Kohn J. Structure-property correlations in a combinatorial library of degradable biomaterials. J. Biomed. Mater. Res. 1998; 42:66–75. [PubMed: 9740008]
29. Gu M, et al. Combinatorial synthesis with high throughput discovery of protein-resistant membrane surfaces. Biomaterials. 2013; 34:6133–6138. [PubMed: 23706542]
30. Bratlie KM, et al. Rapid biocompatibility analysis of materials via *in vivo* fuorescence imaging of mouse models. PLoS One. 2010; 5:e10032. [PubMed: 20386609]
31. Christen T, et al. Molecular imaging of innate immune cell function in transplant rejection. Circulation. 2009; 119:1925–1932. [PubMed: 19332470]
32. Haller J, et al. Visualization of pulmonary infammation using noninvasive fuorescence molecular imaging. J. Appl. Physiol. 2008; 104:795–802. [PubMed: 18202169]
33. Omer A, et al. Survival and maturation of microencapsulated porcine neonatal pancreatic cell clusters transplanted into immunocompetent diabetic mice. Diabetes. 2003; 52:69–75. [PubMed: 12502495]

34. Omer A, et al. Long-term normoglycemia in rats receiving transplants with encapsulated islets. Transplantation. 2005; 79:52–58. [PubMed: 15714169]
35. Veiseh O, et al. Size- and shape-dependent foreign body immune response to materials implanted in rodents and non-human primates. Nat. Mater. 2015; 14:643–651. [PubMed: 25985456]
36. Hofman K, Hall B, Cleaver H, Marshall S. High-throughput quantifcation of hydroxyproline for determination of collagen. Anal. Biochem. 2011; 417:289–291. [PubMed: 21741948]
37. Paredes-Juarez GA, de Haan BJ, Faas MM, de Vos P. A technology platform to test the effcacy of purifcation of alginate. Materials (Basel). 2014; 7:2087–2103.
38. Paredes-Juarez GA, de Haan BJ, Faas MM, de Vos P. The role of pathogen-associated molecular patterns in infammatory responses against alginate based microcapsules. J. Control. Release. 2013; 172:983–992. [PubMed: 24051034]
39. Sato M, et al. Direct binding of Toll-like receptor 2 to zymosan, and zymosan-induced NF-kappa B activation and TNF-alpha secretion are down-regulated by lung collectin surfactant protein A. J. Immunol. 2003; 171:417–425. [PubMed: 12817025]
40. de Vos P, et al. Multiscale requirements for bioencapsulation in medicine and biotechnology. Biomaterials. 2009; 30:2559–2570. [PubMed: 19201460]
41. Orive G, Tam SK, Pedraz JL, Hallé JP. Biocompatibility of alginate-poly-l-lysine microcapsules for cell therapy. Biomaterials. 2006; 27:3691–3700. [PubMed: 16574222]
42. Dusseault J, et al. Evaluation of alginate purifcation methods: effect on polyphenol, endotoxin, and protein contamination. J. Biomed. Mater. Res. A. 2006; 76:243–251. [PubMed: 16265647]
43. Ménard M, et al. Role of protein contaminants in the immunogenicity of alginates. J. Biomed. Mater. Res. B Appl. Biomater. 2010; 93:333–340. [PubMed: 20225212]
44. Madden LR, et al. Proangiogenic scaffolds as functional templates for cardiac tissue engineering. Proc. Natl. Acad. Sci. USA. 2010; 107:15211–15216. [PubMed: 20696917]
45. Brauker JH, et al. Neovascularization of synthetic membranes directed by membrane microarchitecture. J. Biomed. Mater. Res. 1995; 29:1517–1524. [PubMed: 8600142]
46. Liu M, et al. Stabilized hemocompatible coating of nitinol devices based on photo-cross-linked alginate/heparin multilayer. Langmuir. 2007; 23:9378–9385. [PubMed: 17663569]
47. Kim K, Cheng J, Liu Q, Wu XY, Sun Y. Investigation of mechanical properties of soft hydrogel microcapsules in relation to protein delivery using a MEMS force sensor. J. Biomed. Mater. Res. A. 2010; 92:103–113. [PubMed: 19165782]
48. de Haan BJ, et al. Structural surface changes and infammatory responses against alginate-based microcapsules after exposure to human peritoneal fuid. J. Biomed. Mater. Res. A. 2011; 98:394–403. [PubMed: 21630432]
49. Qi M, et al. A recommended laparoscopic procedure for implantation of microcapsules in the peritoneal cavity of non-human primates. J. Surg. Res. 2011; 168:e117–e123. [PubMed: 21435661]
50. Kharb R, Sharma PC, Yar MS. Pharmacological signifcance of triazole scaffold. J. Enzyme Inhib. Med. Chem. 2011; 26:1–21. [PubMed: 20583859]
51. Lindstedt R, et al. The immunosuppressor st1959, a 3,5-diaryl-s-triazole derivative, inhibits T cell activation by reducing NFAT nuclear residency. Int. J. Immunopathol. Pharmacol. 2009; 22:29–42. [PubMed: 19309550]
52. Vegas AJ, et al. Long term glycemic control using polymer-encapsulated human stem cell–derived beta cells in immune-competent mice. Nat. Med. 2016 Jan 25.
53. Stoppel WL, et al. Terminal sterilization of alginate hydrogels: effcacy and impact on mechanical properties. J. Biomed. Mater. Res. B Appl. Biomater. 2014; 102:877–884. [PubMed: 24259507]
54. Bernhardt A, et al. Improved sterilization of sensitive biomaterials with supercritical carbon dioxide at low temperature. PLoS One. 2015; 10:e0129205. [PubMed: 26067982]

References

55. Kang JW, et al. Combined confocal Raman and quantitative phase microscopy system for biomedical diagnosis. Biomed. Opt. Express. 2011; 2:2484–2492. [PubMed: 21991542]

56. Kang JW, Nguyen FT, Lue N, Dasari RR, Heller DA. Measuring uptake dynamics of multiple identifiable carbon nanotube species via high-speed confocal Raman imaging of live cells. Nano Lett. 2012; 12:6170–6174. [PubMed: 23151070]

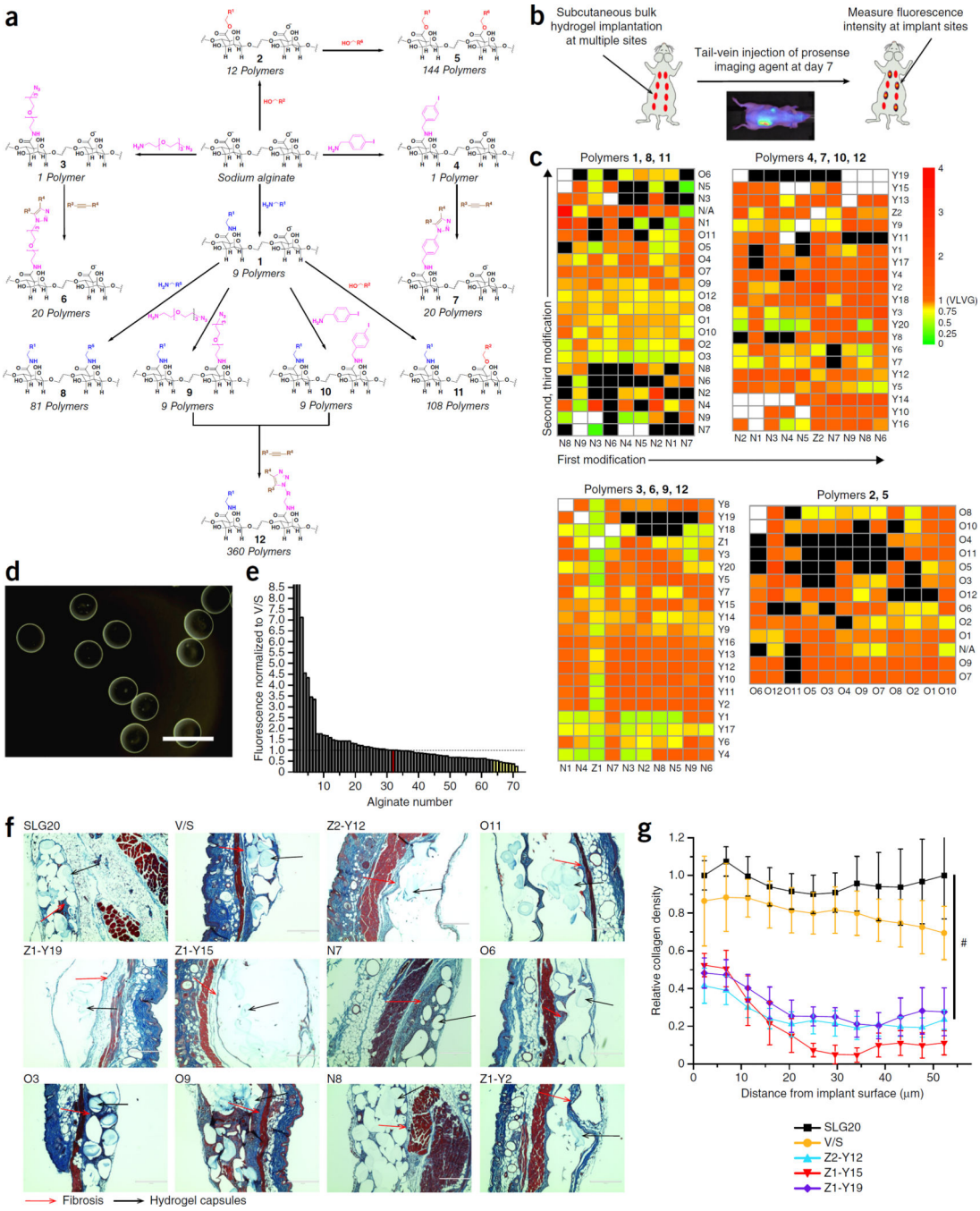

Figure 1.

Combinatorially modified hydrogels with reduced subcutaneous inflammation and fibrosis. (**a**) Scheme for the synthesis of 774 alginate analogs. (**b**) Schematic and representative whole-animal image for the rapid evaluation of multiple analogs as bulk hydrogels implanted subcutaneously in each mouse. The injected Prosense 680 probe is activated by cathepsin activity at implant sites, showing increased fluorescence as a marker of early inflammation. Fluorescence is measured 7 d post-implantation. (**c**) Heat map summarizing gelation and cathepsin evaluation for the entire alginate analog library (mean values from *n*

= 3 replicates for each material). Black (poor gelation) and white (low yield/not created) indicate untested combinations. 200 alginate analogs displayed lower levels of cathepsin activity than the control alginate UPVLVG, the starting material for synthesis. (**d**) Microspheres of alginate analogs formulated using electrojetting. Different alginate analogs were blended with 20–50% SLG100 alginate to produce microcapsules with good spherical morphology. Scale bar, 1,000 μm. (**e**) Secondary cathepsin evaluation of 69 top analogs from the initial screen formulated as 300-μm microcapsules. Data normalized to the fluorescence of V/S microcapsules (V/S = UPVLVG/SLG100 blend; mean values shown). The ten analog microcapsules with the lowest cathepsin levels are highlighted in yellow, $n = 10$ (controls) and $n = 3$ (experimental). (**f**) Masson's trichrome (MT) 28-day subcutaneous histology of the top ten alginate analog microcapsules and the ultrapure control alginate microcapsules (SLG20, V/S = UPVLVG/SLG100 blend) that were implanted in **e**; $n = 10$ (controls) and $n = 3$ (experimental). Abnormal microcapsule morphology is caused by histological processing (dehydration) of the tissue. Scale bars, 400 μm. (g) Quantification of collagen density (blue pixel density) in the MT-stained histology images of the three lead materials shown in **f**; $n = 3$. The collagen density is plotted as a function of the distance from the implant surface to tissue interface (mean values ± s.e.m.). One-way ANOVA with Bonferroni correction was used to allow for statistical comparison of multiple means. $\#P < 0.05$.

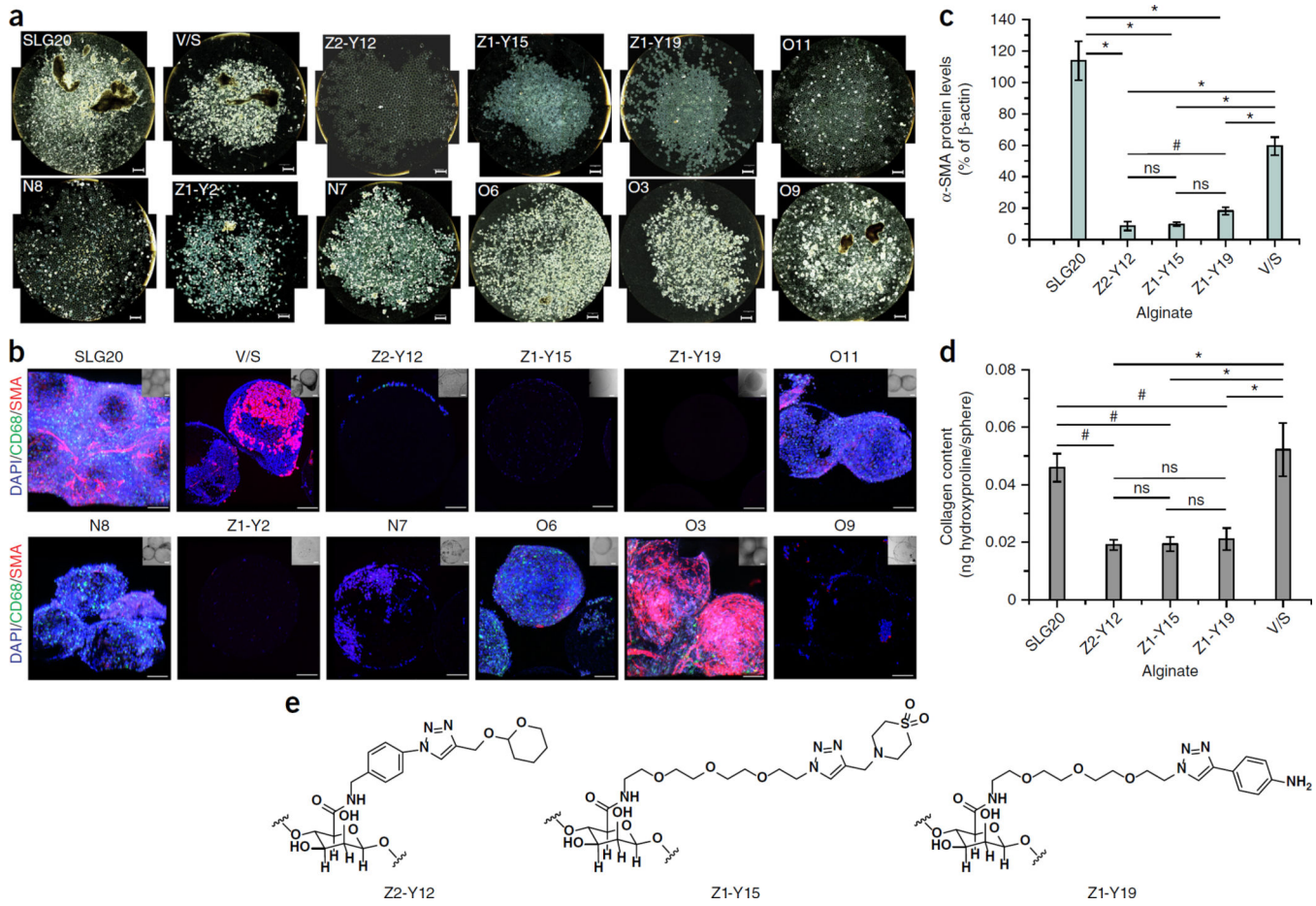

Figure 2.

Three lead hydrogels show reduced fibrosis intraperitoneally in C57BL/6J mice. (**a**) Representative phase contrast images of 300-μm microcapsules of the top ten alginate analog microcapsules and control alginate microcapsules (SLG20, V/S) retrieved from the intraperitoneal space of C57BL/6J mice after 14 d. For each mouse cohort $n = 5$; scale bars, 2,000 μm. (**b**) Representative *z*-stacked confocal microscopy images of the retrieved microcapsules in **a**, $n = 5$. The microcapsules were stained for macrophage markers (CD68), myofibroblast markers (α-smooth muscle actin, SMA) and general cellular deposition (DAPI). Scale bars, 100 μm. (**c**) Western blot analysis of protein extracted from the top three alginate analog microcapsules and control microcapsules in **a**. Blots were stained for SMA and loading was normalized to (β-actin. SMA protein levels determined by quantification of band intensities from the blots shown in Supplementary Figure 2d (mean values ± s.e.m., $n = 5$). One-way ANOVA with Bonferroni correction was used to allow for statistical comparison of multiple means. #$P < 0.05$, *$P < 0.01$; ns, not significant. (**d**) Collagen content using a hydroxyproline quantification assay of protein extracted from the top three alginate analog microcapsules and control microcapsules in **a**, (mean values ± s.e.m., $n = 5$). One-way ANOVA with Bonferroni correction was used to allow for statistical comparison of multiple means. #$P < 0.05$, *$P < 0.01$; ns, not significant. (**e**) Chemical structures of the three lead materials.

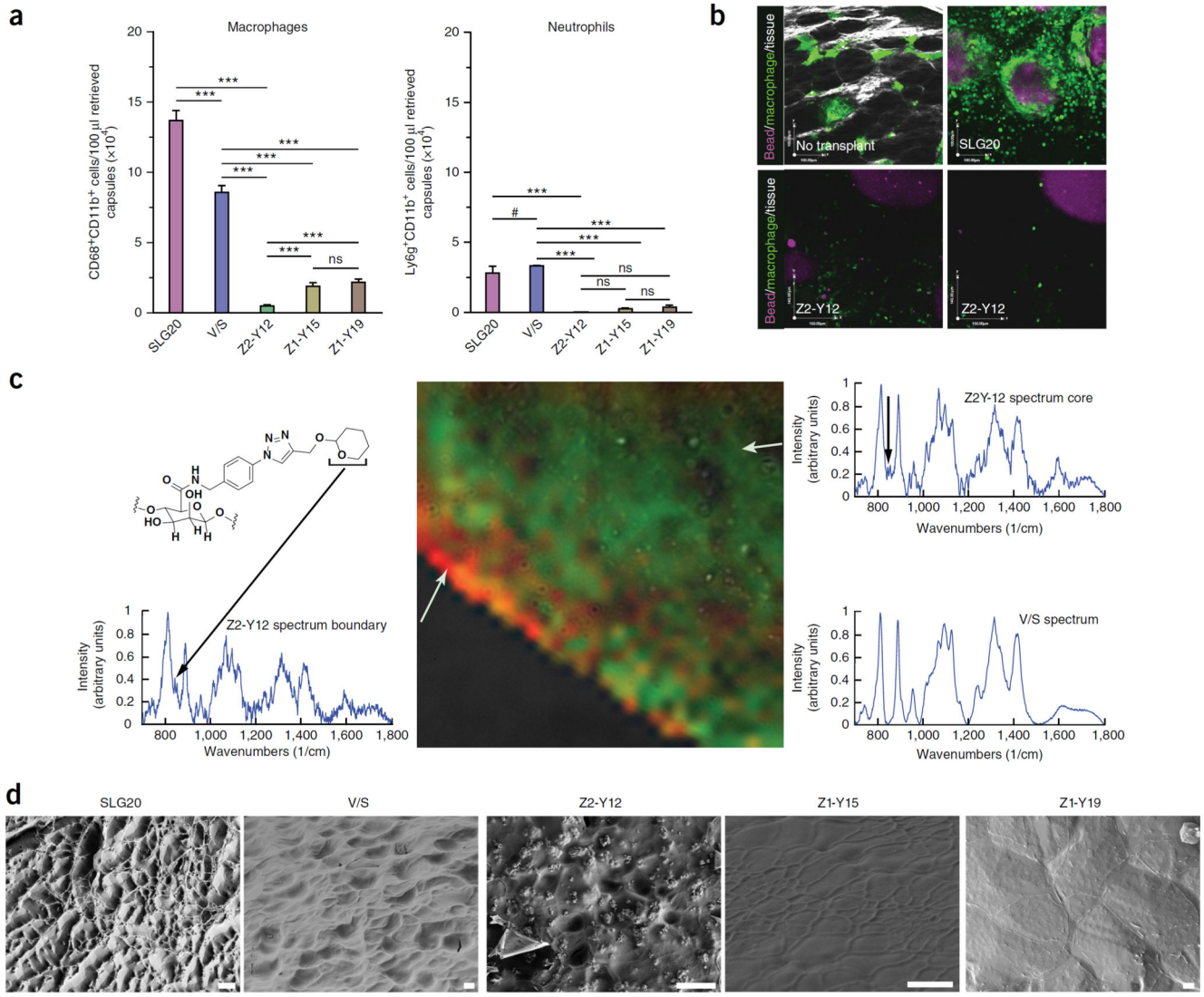

e

Alginate	Percent modification (± s.d.)	Young's modulus, *E* (kPa, ± s.d.)	Surface roughness, P_a (nm, ± s.d.)	Protein adsorption (µg/ml, ± s.d.)
SLG20	–	13.83 (± 2.6)	29.54 (± 7.6)	167.36 (± 8.6)
V/S	–	9.05 (± 3.6)	39.71 (± 10.7)	< 20[a]
Z2-Y12	14.7 (± 3.5)	9.94 (± 3.5)	24.02 (± 1.4)	< 20[a]
Z1-Y15	24.9 (± 3.5)	10.77 (± 3.3)	44.64 (± 8.1)	< 20[a]
Z1-Y19	15.1 (± 6.0)	12.42 (± 2.2)	284.31 (± 89.8)	32.36 (± 3.9)

[a]Below detectable limit of assay

Figure 3.

Lead hydrogels show low immune cell recruitment *in vivo* with covalently modified surfaces. (**a**) FACS analysis of macrophages ($CD11b^+$, $CD68^+$) and neutrophils ($CD11b^+$, $Ly6g^+$) isolated from Z2-Y12, Z1-Y15, Z1-Y19, SLG20 and V/S microcapsules retrieved after 14 d in the intraperitoneal space of C57BL/6J mice, $n = 5$. One-way ANOVA with Bonferroni correction was used to allow for statistical comparison of multiple means. #$P < 0.05$; ***$P < 0.0001$. (**b**) Intravital imaging and single *z*-sections of fluorescent 300-µm Z2-Y12 and SLG20 microcapsules in MAFIA mice 7 d after implantation ($n = 3$). Green, GFP-

expressing macrophages; red, fluorescent hydrogel microcapsules. For full confocal reconstructions, see Supplementary Videos 1 and 2. (**c**) Confocal Raman cross-section mapping of 300-μm Z2-Y12 microcapsules. The Raman peak at 830 cm^{-1} (shown in red) is indicative of the tetrahydropyranal modification of Z2-Y12, and the intensity of this peak is two times higher at the surface of the microcapsules than at the core. The peak at 1,000 cm^{-1} is mapped in green as a reference to the alginate backbone structure. The Raman spectrum of V/S microcapsules is also shown for reference. (**d**) Freeze-fracture cryo-SEM imaging of 300-μm Z2-Y12, Z1-Y15, Z1-Y19, V/S and SLG20 microcapsules. Representative images of the microcapsule surface topography is shown. Scale bars, 3 μm. (**e**) Table reporting percent polymer modification (n = 3, mean values ± s.d.), Young's modulus (n = 5, mean values ± s.d.), surface roughness (n = 3, mean values ± s.d.) and protein adsorption (n = 8, mean values ± s.d.) for the three lead materials and controls.

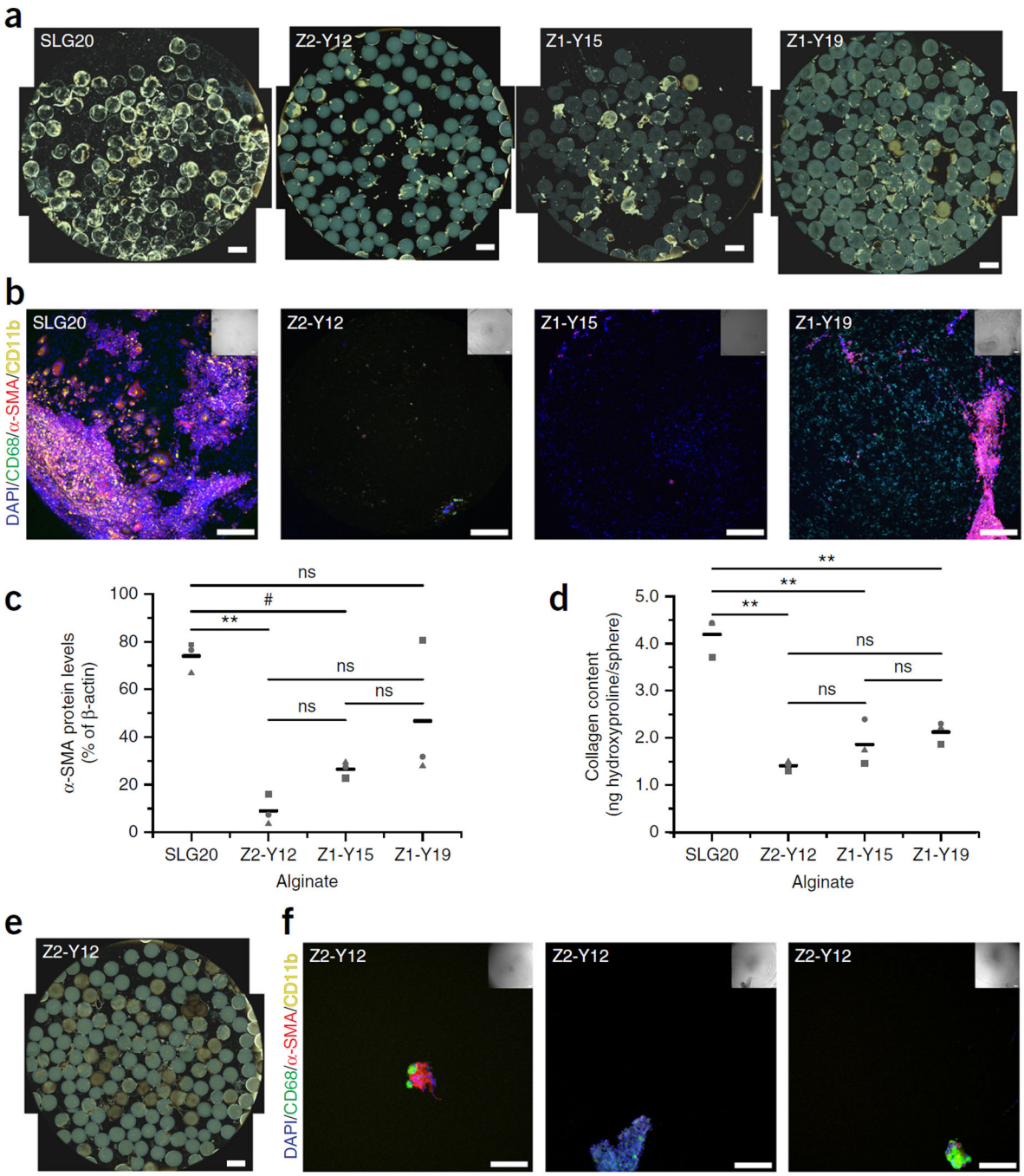

Figure 4.

Lead hydrogels mitigate the foreign body response in non-human primates. Z2-Y12, Z1-Y15, and Z1-Y19 spheres significantly reduce fibrosis in cynomolgus macaques, while conventional SLG20 spheres become fibrotic. (**a**) Phase contrast imaging of spheres retrieved after 4 weeks in the intraperitoneal space show less fibrosis on Z2-Y12, Z1-Y15 and Z1-Y19 spheres than on SLG20. Scale bars, 2,000 μm; $n = 3$. (**b**) Confocal imaging of retrieved spheres from a after 4 weeks in the intraperitoneal space show significantly less macrophage (CD68, CD11b), myofibroblast (SMA) and general cellular deposition (DAPI)

on Z2-Y12 spheres. Scale bars, 200 μm; $n = 3$. Brightfield images of the stained spheres are inset; scale bars, 100 μm. (**c**) Western-blot analysis of protein extracted from the top three alginate analog spheres and control spheres in **a**; $n = 3$. Blots were stained for SMA and loading was normalized to β-actin. SMA protein levels determined by quantification of band intensities from the blots shown in Supplementary Figure 7b. Dots represent measurements from individual biological replicates, and lines show the average of the three replicates. One-way ANOVA with Bonferroni correction was used to allow for statistical comparison of multiple means. $\#P < 0.05$; $**P < 0.001$; ns, not significant. (**d**) Collagen content using a hydroxyproline quantification assay of protein extracted from the top three alginate analog spheres and control spheres in **a**; $n = 3$. Dots represent measurements from individual biological replicates and lines show the average of the three replicates. One-way ANOVA with Bonferroni correction was used to allow for statistical comparison of multiple means. $\#P < 0.05$, $**P < 0.001$, ns = not significant. (**e**) Representative phase contrast imaging ($n = 3$) of Z2-Y12 after 6 months in the intraperitoneal space. Scale bar, 2,000 μm. (**f**) Representative *z*-stacked confocal imaging ($n = 3$) of Z2-Y12 spheres retrieved after 6 months. Few macrophages and myofibroblasts are observed on Z2-Y12 spheres. Scale bars, 200 μm.